# Molecular-dynamics study of the high-temperature elasticity of quartz above the $\alpha$-$\beta$ phase transition

Hajime Kimizuka*
*Energy & Environment Technology Group, Science Division, The Japan Research Institute Limited, Tokyo 102-0082, Japan*

Hideo Kaburaki
*Center for Promotion of Computational Science and Engineering, Japan Atomic Energy Research Institute, Ibaraki 319-1195, Japan*

Yoshiaki Kogure
*Faculty of Science and Engineering, Teikyo University of Science & Technology, Yamanashi 409-0193, Japan*
(Received 15 October 2002; published 16 January 2003)

We have presented the molecular-dynamics (MD) results for the temperature dependence of the adiabatic elastic constants $C_{ij}$ of $\alpha$ and $\beta$ quartz, using a statistical fluctuation formula. It is noteworthy that the calculated $C_{ij}$ values are in a good agreement with the experimental values in the entire temperature range of 300–1100 K, including the $\alpha$-$\beta$ phase-transition region. We have confirmed that the net increase of bulk $C_{ij}$'s in the $\beta$ phase can be attributed to the internal relaxations, which arise from the cooperative motions of corner-linked $SiO_4$ tetrahedra. Our MD simulations have revealed the existence of dynamical disorder in $\beta$ quartz at high temperatures, and its influence on the macroscopic elastic properties, in contrast to the ordered $\beta$-quartz structure model.

DOI: 10.1103/PhysRevB.67.024105 PACS number(s): 62.20.Dc, 64.70.Kb

## I. INTRODUCTION

Quartz, which is one of the low-pressure polymorphs of $SiO_2$, has received much attention in diverse fields due to its technological and geophysical importance. The low-temperature $\alpha$ form of quartz undergoes a structural phase transition to the high-temperature $\beta$ form at 847 K with minor changes in the silicon and oxygen sites. Despite the number of experimental and theoretical studies of the $\alpha$-$\beta$ structural phase transition and related phenomena in quartz, its microscopic nature has not yet been completely clarified. The $\alpha$-$\beta$ transition induces the marked changes in various physical and thermodynamic properties, in particular, elastic properties. The exact nature of the changes in elastic properties with temperature has been the subject of long controversies on the microscopic mechanisms of the transition and the microscopic nature of $\beta$-quartz structure.

Numerous ultrasonic and Brillouin scattering experiments have been conducted to measure elastic properties of quartz crystal near the phase transition between $\alpha$ and $\beta$ phases.[1] In order to explain the temperature dependence of the elastic constant based on the experimental values, the Landau-free-energy expansion method is often employed and is expected to provide a valid description of the macroscopic behavior over many hundred degrees away from the transition point (see, for example, Ref. 2). The description of the transition dependent properties can be correlated by an order parameter introduced according to the Landau theory of phase transition with symmetry change; however, the phenomenological approach does not make any mention of the microscopic mechanism for the transition.

On the other hand, atomistic simulations have been carried out to clarify the microscopic nature of quartz related to the $\alpha$-$\beta$ transition. Smirnov and Mirgorodsky[3] have recently performed lattice-dynamical calculations using the pairwise potential by Tsuneyuki *et al.*[4] Their model provides good results on the elastic properties of $\alpha$ quartz, but fails to predict the data of $\beta$ quartz. They assumed an ideal hexagonal structure of $\beta$ quartz in the calculation, and concluded that this structure is not compatible with the measured elasticity. Compared with the lattice-dynamics method, molecular-dynamics (MD) simulations are expected to treat large fluctuations in the atomic motions inherent in the critical phenomena. To our knowledge, a systematic explanation has not been available on the elastic properties of $\beta$ quartz observed above the transition temperature. The main objective of the present paper is to provide results of the MD simulations that can be used to evaluate quantitatively the high-temperature elasticity of quartz, and to investigate the nature of dynamical disorder present in the $\beta$ phase and its influence on the microscopic mechanism for the elastic-constant behavior associated with the $\alpha$-$\beta$ phase transition.

## II. NATURE OF HIGH-TEMPERATURE PHASE

It is well known that $\alpha$ quartz with trigonal symmetry transforms into the hexagonal $\beta$ phase via a displacive transition at 847 K. The structure of $\alpha$ quartz is described by the space group $P3_121$ (or the enantiomorphic one $P3_221$), and that of $\beta$ quartz $P6_222$ (or $P6_422$). Both $\alpha$ and $\beta$ quartz have three $SiO_2$ groups in hexagonal unit cells with almost the same dimensions, consisting of corner-sharing $SiO_4$ tetrahedra placed in right or left helix around the crystallographic $c$ axis. The $\alpha$ and $\beta$ phases differ only slightly in the relative orientations of the $SiO_4$ units.

One of the important symmetry-dependent properties is twinning. In the $\alpha$ phase, there exist two potential minima $\alpha_1$ and $\alpha_2$ called the Dauphiné twins. It is known that twinning is produced in the $\alpha$ phase either during crystal growth

 

or under the action of external fields (local stresses, thermal shock, etc.). The crystal structures of $\alpha_1$ and $\alpha_2$ are specified by the atomic coordinates $[\mathrm{Si}(u,0,0),\mathrm{O}(x,y,z)]$ and $[\mathrm{Si}(1-u,0,0),\mathrm{O}(x,x-y,\frac{1}{3}-z)]$, respectively. The saddle point $\beta$ $[\mathrm{Si}(\frac{1}{2},0,0),\mathrm{O}(x',x'/2,\frac{1}{6})]$ lies midway between $\alpha_1$ and $\alpha_2$. This twinning is closely related to the $\alpha$-$\beta$ transition because of the experimental fact that the Dauphiné twinning disappears in the $\beta$ phase. In particular, the Dauphiné twinning, corresponding to the orientation of the $OX$ axis (which becomes polar in the $\alpha$ phase), changes the sign of the piezoelectric constant $d_{11}$ ($d_{xxx}$) and the elastic constant $C_{14}$ ($C_{xxyz}$) but does not affect the other components.[5]

In connection with this Dauphiné twinning, there is still a discussion on the nature of the high-temperature $\beta$ phase despite a long history of investigations. Young[6] examined the structure with x-ray diffraction and concluded that $\beta$ quartz was a normal ordered structure. Wright and Lehmann[7] in their neutron-diffraction studies, however, favor a disordered model, in which atoms are distributed over two positions corresponding to the Dauphiné twinning. The static-lattice-energy calculations[3] presented a picture of the potential-energy curves along the $\alpha_1$-$\beta$-$\alpha_2$ path close to the transition. As the unit-cell volume exceeds the critical value, the double-well potential structure transforms smoothly into a broad single-well one. Here, they considered the ideal $\beta$-quartz structure obtained by experiments.

If we assume the actual crystal structure is of a dynamically averaged character, the question is whether (i) the atoms in the $\beta$ phase vibrate around the idealized positions or (ii) the atoms are disordered between two positions corresponding to the Dauphiné twinning, and vibrate to and fro between the two minima. Tsuneyuki *et al.*[4] investigated the microscopic nature of the anharmonicity in the $\beta$-quartz structure, and they pointed out that whether $\beta$ quartz has a dynamical average structure or a disordered structure of $\alpha_1$ and $\alpha_2$ domains, it depends on the time and length scales as a function of temperature. We verify this view by observing the macroscopic elastic properties and other dynamical properties using the MD simulations.

## III. COMPUTATIONAL METHOD

### A. Molecular-dynamics simulations of $\alpha$ and $\beta$ quartz

The equilibrium MD simulations of quartz have been performed starting from the low-temperature $\alpha$ phase at 300 K to the high-temperature $\beta$ phase continuously across the transition point. The Nosé-Hoover[8] and the Parrinello-Rahman[9] isobaric-isothermal thermostat is applied to realize the structures of the reference states at 300–1400 K under zero external stress. In constructing the initial configurations of $\alpha$ quartz, atoms are placed on the experimentally determined positions (see Ref. 7). The temperature of the system is continuously raised up to the desired value at a rate of 25 K/ps, after which the system is equilibrated over 80 ps. The integration time step in all the MD simulations is 2 fs.

We have employed the effective pairwise potential by van Beest, Kramer, and van Santen[10] (BKS) derived from the cluster calculations of potential-energy surfaces using the *ab initio* method. The interatomic potential is expressed as

$$u(r_{ab})=\frac{z_a z_b e^2}{r_{ab}}+a_{ab}\exp(-b_{ab}r_{ab})-\frac{c_{ab}}{r_{ab}^6}, \qquad (1)$$

where $u(r_{ab})$ is the interaction energy between atoms $(a,b)$, $r_{ab}$ is the interatomic separation, and ($z_a$, $z_b$, $a_{ab}$, $b_{ab}$, $c_{ab}$) are parameters fitted to Hartree-Fock calculations for a $H_4SiO_4$ molecule and experimental data for crystalline silica (such as structural and elastic properties). Despite its simplicity, their force-field parameters are reasonably successful in describing the structural and dynamical properties of $SiO_2$.

The numbers of atoms in the periodic hexagonal simulation boxes are 576 and 4608, containing $64(=4\times4\times4)$ and $512(=8\times8\times8)$ unit cells, respectively. Here, the simulations in this paper were basically carried out with the system of 576 atoms, while the system of 4608 atoms was adopted to study in detail the phase-transition region. The Coulomb interactions are calculated using the Ewald method. The long-range corrections in the calculated stress[11] are taken into account to reduce the errors introduced by the truncation of the interactions at the cutoff radius $r_c$ for the non-Coulombic interactions in Eq. (1). Since the potential surface of quartz is sensitive to the volume change,[3,4] this correction $P_c$ affects the transition temperature, especially in the small system. In the 576-atom system ($r_c$ = about 10.0 Å), the transition temperature shifts from ca. 700 to 825 K due to the correction ($P_c=-0.55$ GPa). However, in the 4608-atom system ($r_c=$ about 17.5 Å), the transition temperature is observed to be ca. 900 K, irrespective of the adoption of this correction ($P_c=-0.09$ GPa).

### B. Calculation of elastic constants

The adiabatic elastic constants at various temperatures were calculated within the constant-volume and constant-energy ensemble. The fluctuation formula for the internal stress tensor[12] was used to obtain a complete set of elastic constants over a wide temperature range. The elastic constants under conditions of zero stress at a finite temperature are expressed by

$$C_{ijkl}=-\frac{V_0}{k_BT}\delta(P_{ij}P_{kl})+\frac{2Nk_BT}{V_0}(\delta_{il}\delta_{jk}+\delta_{ik}\delta_{jl}) + \frac{1}{V_0}\left\langle\sum_{b>a} f(r_{ab})x_{abi}x_{abj}x_{abk}x_{abl}\right\rangle_{\mathrm{av}}. \qquad (2)$$

Here, $P_{ij}$ denotes the internal stress tensor, $x_{ab}$ the vector joining $a$ and $b$ of length $r_{ab}$, $V_0$ the volume containing the $N$ particles, and $f=r^{-2}(u''-r^{-1}u')$, where the pair potential is denoted by $u(r)$. The fluctuation of a product of $A$ and $B$ is defined by $\delta(AB)=\langle AB\rangle_{\mathrm{av}}-\langle A\rangle_{\mathrm{av}}\langle B\rangle_{\mathrm{av}}$, where the bracket represents the ensemble-average value. In order to check the validity of statistical sampling, the averages are separately taken every 80 ps during a 1.28-ns run for each temperature.

TABLE I. Adiabatic elastic constants (in GPa) of $\alpha$ and $\beta$ quartz.

| | $\alpha$ quartz (300 K) | | $\beta$ quartz (900 K) | |
|---|---|---|---|---|
| | Present study | Expt.[a] | Present study | Expt.[b] |
| $C_{11}$ | 93.0 | 86.7 | 123.4 | 118.4 |
| $C_{33}$ | 108.4 | 107.2 | 111.4 | 107.0 |
| $C_{44}$ | 50.3 | 57.9 | 33.4 | 35.8 |
| $C_{66}$ | 40.7 | 39.8 | 47.7 | 49.7 |
| $C_{12}$ | 10.0 | 7.0 | 27.3 | 19.0 |
| $C_{13}$ | 17.9 | 11.9 | 40.6 | 32.0 |
| $C_{14}$ | 15.9 | 17.9 | −0.2 | |

[a]Reference 14.
[b]Reference 15.

The right-hand side of Eq. (2) consists of three separate terms; the stress-fluctuation term, the kinetic term, and the Born term. In this formula, a significant contribution to the total elastic constants comes from both the Born term and the stress-fluctuation term. The Born term is described by the interatomic potential and the atomic coordinates, and the static limit of this term represents the elastic constants at zero temperature for the primitive Bravais lattice with no internal strain. When there is more than one atom present in the primitive unit cell, internal strains occur within the cell, and thus give rise to a relaxation contribution to the elastic constants. Using the fluctuation formula, the effect of internal strain relaxation is described by the stress-fluctuation term through the MD simulations. To calculate the elastic constants, in particular, for the $SiO_2$ phases, the MD method with the fluctuation formula has an advantage over the harmonic lattice-dynamics method, in which the results contain the anharmonic and finite-temperature effects in an exact manner (see, for example, Ref. 13).

## IV. RESULTS AND DISCUSSION

### A. Temperature evolution of elastic constants

The adiabatic elastic stiffness constants ($C_{ij}$; we use the Voigt compressed notation to denote the fourth-rank tensors.) of quartz were calculated using the MD method, while the dynamical structures above the transition are directly taken into account in the simulations. The obtained $C_{ij}$ values are given in Table I. We confirm that the absolute values of the $C_{ij}$'s are well described by the BKS potential, even in the high-temperature region above the transition point. Figure 1 shows the temperature dependence of the $C_{ij}$'s of quartz using this potential. The experimental $C_{ij}$ values from 300 to 1100 K are also shown in Fig. 1 (data from Ref. 1). In Fig. 1, the $C_{11}$, $C_{33}$, $C_{12}$, and $C_{13}$ exhibit a sharp dip in the temperature region of 800–825 K, which clearly indicates the occurrence of the phase transition, and they rapidly recover with temperature in the $\beta$ phase region. On the contrary, $C_{44}$ and $C_{66}$ change little over the transition point. It is noteworthy that the temperature dependence of the calculated $C_{ij}$'s are also found to agree very closely with experiment, in the entire temperature range of 300–1100 K. Besides, the elastic

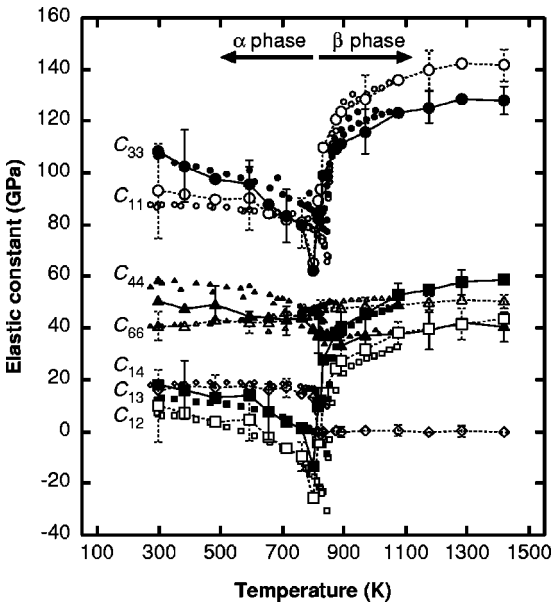


FIG. 1. Evolution with temperature of the adiabatic elastic constants of quartz. The symmetry of the trigonal $\alpha$ form leads to six independent components; $C_{11}$ (open circle), $C_{33}$ (solid circle), $C_{44}$ (solid triangle), $C_{12}$ (open square), $C_{13}$ (solid square), and $C_{14}$ (open diamond). Here, $C_{66}$ (open triangle) coincides with $(C_{11}-C_{12})/2$. The ultrasonic and Brillouin scattering experimental data (small symbols) are from Ref. 1.

constant $C_{14}$ tends to be zero as the temperature approaches the transition point and vanishes in the $\beta$ phase. This fact demonstrates clearly that the symmetry of the crystal system determined by the atomic coordinates alters from trigonal to hexagonal across the transition point in the similar hexagonal lattices.

In Fig. 2, we show contributions to the total elastic constants of quartz from two terms in Eq. (2), i.e., the Born term and the stress-fluctuation term, as a function of temperature. The constant kinetic terms are ignored here, since they are orders of magnitude smaller. We can see a marked difference between the two terms in their temperature evolution of $C_{11}$ and $C_{33}$; the Born terms decrease steadily in the $\alpha$ phase as the temperature approaches the transition point, and become almost constant in the $\beta$ phase. On the other hand, the stress-fluctuation terms exhibit a sudden drop and a sharp rise after the transition, and grow steadily in the $\beta$ phase. We find that the contributions to the $C_{ij}$'s in the fluctuation formula are dominated by the Born term in the $\alpha$ phase and by the stress fluctuation term in the $\beta$ phase. This demonstrates that the internal strain relaxation of atoms within the cell, which is evaluated from the stress-fluctuation term, plays an important role in the macroscopic elasticity of quartz in the high-temperature region. From the MD results concerning the radial distribution function and the angle distribution function, we confirm that the rigid $SiO_4$ tetrahedral units are maintained through the transition. Despite the large stiffness of tetrahedral units, the flexible framework structures readily undergo volumetric deformation through cooperative $SiO_4$ rotations, due to the weak potentials between $SiO_4$ tetrahe-

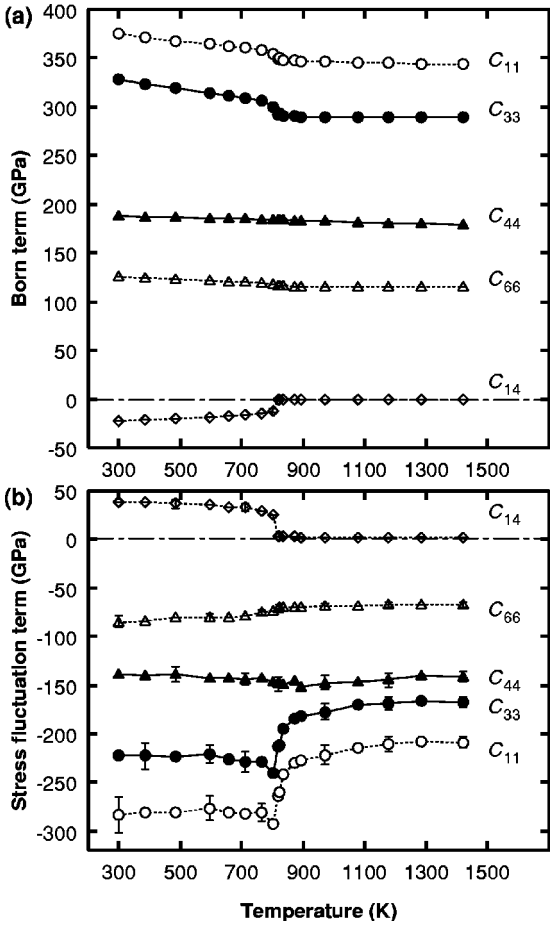


FIG. 2. The Born-term (a) and stress-fluctuation-term (b) contributions to the adiabatic elastic constants of quartz as a function of temperature.

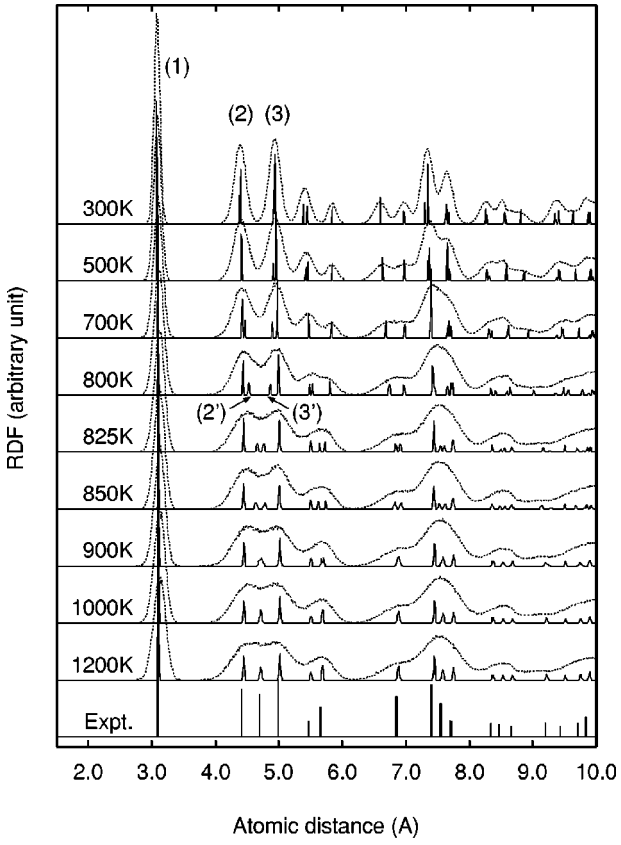


FIG. 3. The RDF of quartz for Si-Si distance (dashed lines). The RDF's of the time-averaged structures (solid line) are normalized by a factor of 20, for the sake of appearance. The RDF of the ideal $\beta$-quartz structure (Expt.) is derived from the experimental data from Ref. 13.

dra. We suggest here that intrinsic changes in the stress fluctuations be attributed to these cooperative motions of corner-linked $SiO_4$ tetrahedra.

### B. Structural changes across the transition

To obtain information about the organization and dynamics of neighboring $SiO_4$ tetrahedra, the radial distribution functions (RDF) for Si-Si distances in quartz are shown in Fig. 3, at various temperatures (dashed lines). The RDF's for the time-averaged structures (over 20 ps) are also shown (solid line), which indicate the average Si-Si distances evaluated from the center of motions of silicon atoms.

In Fig. 3, we observe that the $\alpha$ phase continuously evolves into the $\beta$ phase close to the transition. The peaks, which indicate medium-range order beyond the nearest-neighbor silicon atoms, become much broader as the temperature increases. This indicates that $SiO_4$ tetrahedral positions are less ordered in $\beta$ quartz due to the dynamical motions of $SiO_4$ units. In particular, while the first-nearest Si-Si distance (peak 1) is not significantly affected by the transition, the second- and third-nearest ones (2 and 3) exhibit distinctive evolution. As the temperature increases, the peaks 2 and 3 split separately, and thus two subpeaks $(2')$ and $(3')$ emerge. They approach each other close to the $\alpha$-$\beta$ transition, and eventually merge together in the $\beta$ phase. This fact clearly shows that the phase transforms into the higher-symmetry one (Fig. 4). Also, the peaks for the time-averaged structure of the $\beta$ phase agree well with those of the experiment concerning the ordered model of the $\beta$-quartz structure.[6,7] According to the symmetrical consideration, one

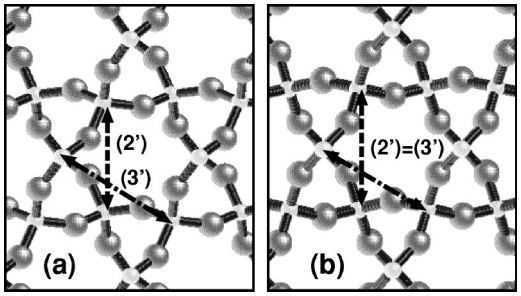


FIG. 4. Framework structure of $\alpha$ quartz (a) and ideal $\beta$ quartz (b), viewed down the common [001] direction. The oxygen and silicon atoms are represented by the large and small spheres, respectively. In the low-symmetry $\alpha$ phase, the Si-Si distance, $2'$ is shorter than $3'$, and the structure exhibits trigonal symmetry. On the other hand, the ideal $\beta$-quartz structure has the $SiO_4$ tetrahedra aligned to form rings of perfect sixfold symmetry, so that $2'=3'$.

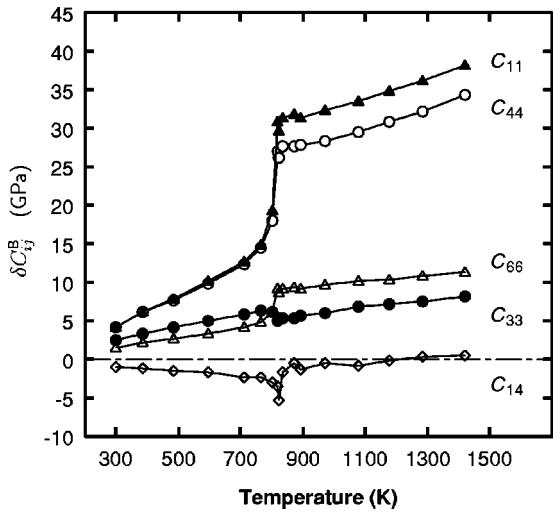


FIG. 5. Temperature dependence of the difference between the Born terms, evaluated from the time-averaged (ordered) structures and instantaneous (disordered) structures, respectively ($\delta C_{ij}^{\mathrm{B}} = C_{ij}^{\mathrm{B(av)}} - C_{ij}^{\mathrm{Born}}$).

can distinguish the $\alpha$ and $\beta$ phases from the shape of the merged peaks (double or single ones). It is noteworthy that (not the single) the double peaks clearly remain at 825–900 K, which is higher than the transition point estimated from the discontinuous jump of $C_{ij}$ values (at ca. 800–825 K). It indicates that, in the 576-atom system, $\alpha$ phases ($\alpha_1$ or $\alpha_2$) can survive even temporarily (over several tens of picoseconds) just above the transition temperature. (The $\alpha_1$ and $\alpha_2$ phases cannot be distinguished from the RDF's because the relative Si-Si distances are equivalent between them.) This fact is related to the dynamical motions of $SiO_4$ tetrahedra along the $\alpha_1$-$\beta$-$\alpha_2$ path, in the close vicinity of the transition point.

### C. Elastic properties based on the ideal $\beta$-quartz structure

In order to examine the dynamical effects of atoms on the elastic properties, the temperature dependence of the Born-term contribution is compared with that for the ideal $\beta$-quartz geometry obtained from the time-averaged structures, as shown in Fig. 3 for the RDF's. The original Born term $C_{ijkl}^{\mathrm{Born}}$, which is averaged over the instantaneous values $C_{ijkl}^{\mathrm{B(ins)}}$, and the static Born term, which is evaluated from the static calculation for the time-averaged structures, are represented as

$$C_{ijkl}^{\mathrm{Born}} = \langle C_{ijkl}^{\mathrm{B(ins)}} \rangle = \frac{1}{V_0} \left\langle \sum_{b>a} f(r_{ab}) x_{abi} x_{abj} x_{abk} x_{abl} \right\rangle, \tag{3}$$

$$C_{ijkl}^{\mathrm{B(av)}} = \frac{1}{V_0} \sum_{b>a} f(\langle r_{ab} \rangle) \langle x_{abi} \rangle \langle x_{abj} \rangle \langle x_{abk} \rangle \langle x_{abl} \rangle. \tag{4}$$

Here, it is apparent that $C_{ij}^{\mathrm{Born}}$ and $C_{ij}^{\mathrm{B(av)}}$ coincide at zero temperature.

Figure 5 shows the temperature evolution of the difference $\delta C_{ij}^{\mathrm{B}} = C_{ij}^{\mathrm{B(av)}} - C_{ij}^{\mathrm{Born}}$, evaluated from the MD simulations. When the equilibrium positions of atoms in the actual $\beta$-quartz structure coincide with the ideal (time-averaged) lattice points, the $\delta C_{ij}^{\mathrm{B}}$ value is expected to exhibit a uniform evolution with temperature. However, the differences, in particular, for the $C_{11}$ and $C_{44}$ components increase significantly above the transition point at $\approx$850 K. As a result, the calculated elastic constants based on the ideal $\beta$-quartz structure are considerably overestimated, compared with the measured values.

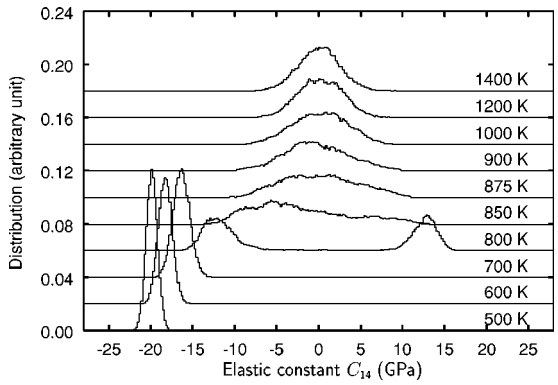


FIG. 6. Histograms of $C_{14}^{\mathrm{B(ins)}}$ over the 50 000 time step calculation (100 ps) for the 576-atom system, plotted against temperature. Double peaks observed at 800 K are due to the fictitious phase fluctuation between two potential minima $\alpha_1$ and $\alpha_2$, owing to the finite-size effect of the system.

We suggest that the actual sites of atoms in $\beta$ quartz be dynamically disordered and the framework of $SiO_4$ tetrahedra show a rotation at the corner-linked points at each instant, due to the effect of the internal strain relaxation. We have confirmed in the present MD picture that the ideal $\beta$-phase geometry is not compatible with the elastic properties observed above transition temperature, and the local structure of $\beta$ quartz is distinct from the ordered structure with the atoms vibrating isotropically about their mean (idealized) positions.

### D. Dauphiné twinning and phase-mixing behavior

The finite elastic constant $C_{14}$ is characteristic of $\alpha$ quartz in the trigonal system in contrast to $C_{14}=0$ for $\beta$ quartz with hexagonal symmetry. Also, in relation to the Dauphiné twinning, the twinned part is given by an operation of rotation $\pi$ along the $c$ axis, so that the value of $C_{14}$ in the twinned part is that with a sign reversed, $-C_{14}$. Following the Landau theory, one can introduce an order parameter $\eta$ that is zero in the $\beta$ phase, and takes two opposite values in the $\alpha$ phase, corresponding to the Dauphiné twinning. Several quantities, such as $C_{14}$, are known to change as $\eta$. The behavior of $C_{14}$ in association with the phase transition should give the information on the microscopic nature of the heterogeneity in the $\beta$-quartz structure.

Figure 6 shows the histograms of $C_{14}^{\mathrm{B(ins)}}$, whose average corresponds to the Born-term contribution to the elastic constant $C_{14}$, over the 50 000 time step calculation at various temperatures. In the $\alpha$ phase ($<$850 K), the $C_{14}^{\mathrm{B(ins)}}$ value remains finite, and the center of the distribution approaches

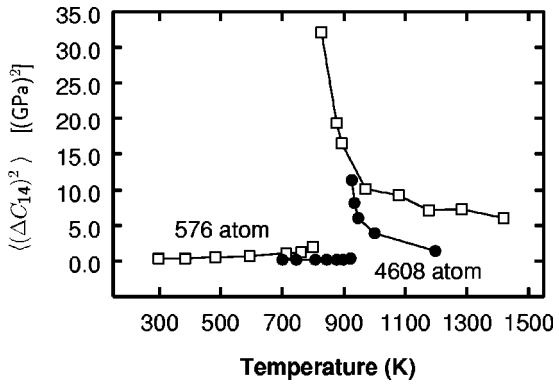


FIG. 7. Temperature evolution of the variance of the distribution $\langle(\Delta C_{14}^{\mathrm{B(ins)}})^2\rangle$, for the 576-atom (open square) and 4608-atom systems (solid circle).

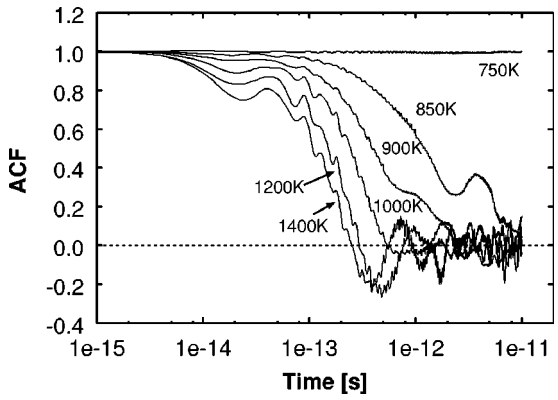


FIG. 9. Time autocorrelation functions of $C_{14}^{\mathrm{B(ins)}}$ at various temperatures.

zero as the temperature increases. After the transition, the $C_{14}^{\mathrm{B(ins)}}$ value begins to fluctuate around zero ($\langle C_{14}^{\mathrm{B(ins)}}\rangle = 0$). Here, the heterogeneity in the $\beta$-quartz phase shows up as a broad and non-bell-shaped distribution, especially in the close vicinity of the transition point. Figure 7 shows the temperature evolution of the variance of the distribution $\langle(\Delta C_{14}^{\mathrm{B(ins)}})^2\rangle$, where the fluctuation is denoted by $\Delta C_{14}^{\mathrm{B(ins)}} = C_{ij}^{\mathrm{B(ins)}} - \langle C_{ij}^{\mathrm{B(ins)}}\rangle$. The prominent spread is observed at around the transition point, and it indicates that the presence of the critical fluctuations, which is associated with the dynamics along the $\alpha_1$-$\beta$-$\alpha_2$ path, makes the phase unstable in the vicinity of the transition point, and thus triggers the structural phase transition.

To examine the microscopic nature of the anharmonicity in the $\beta$-quartz structure, we define the non-Gaussian parameter of $C_{14}^{\mathrm{B(ins)}}$, which is expressed by

$$U_L = \langle (C_{14}^{\mathrm{B(ins)}})^4\rangle / \langle (C_{14}^{\mathrm{B(ins)}})^2\rangle^2. \tag{5}$$

The parameter $U_L$ is equal to 3.0 if the distribution of $C_{14}^{\mathrm{B(ins)}}$ is Gaussian and its mean exhibits zero (for the $\beta$ phase), which indicates that the $\alpha_1$ and $\alpha_2$ phase-mixing behavior is homogeneous and random (statistically independent), while $U_L$ is equal to 1.0 if its mean exhibits nonzero value (for the $\alpha_1$ or $\alpha_2$ phase). Figure 8 shows the temperature dependence

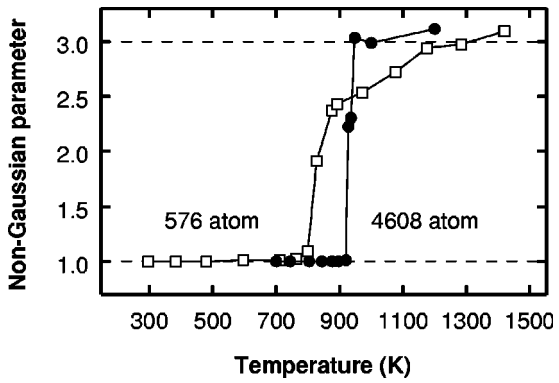


FIG. 8. Temperature evolution of the non-Gaussian parameter of $C_{14}^{\mathrm{B(ins)}}$, for the 576-atom (open square) and 4608-atom systems (solid circle).

of $U_L$'s obtained for the 576- and 4608-atom systems. We can see that $U_L$ changes from 1.0 to 3.0 in both systems across the phase transition. The intermediate region between the two bounds indicates the existence of heterogeneous structures produced by the Dauphiné twinning and phase mixing. Although the distribution of $C_{14}$ approaches clearly and abruptly to the Gaussian in the 4608-atom system, the heterogeneous disordered structure survives even in the high-temperature region in the 576-atom system due to the limitation in size. It suggests that the 4608-atom system would be able to sufficiently hold the domain walls, whereas the 576-atom system would not be large enough to capture fluctuations in this transition-temperature region. Thus, the domain size of $\alpha_1$ and $\alpha_2$ phase mixing is of the order of unit cells at the most ($\leqslant$576-atom system), and the length scales of these domains become smaller with increasing temperature. Also, locally, the structure of $\beta$ quartz looks similar to that of the $\alpha$ phase on the scale of the unit-cell size, albeit with the dynamic switching between different orientations of the polar directions ($\alpha_1$ and $\alpha_2$). The larger system sharply approaches a more homogeneous structure with temperature, since the system can hold a lot of small domains, to give a structure that is averaged over all domains and, therefore, has the appearance of the high-symmetry structure. Eventually, the domain walls vanish in the higher-temperature region, and the homogeneous $\beta$ phase is realized as a dynamically averaged structure.

In order to follow up a dynamical picture of the $\beta$-quartz structure, time autocorrelation functions (ACF) of $C_{14}^{\mathrm{B(ins)}}$ are calculated at various temperatures (Fig. 9). We clearly observe that while the phase maintains a high degree of correlation before the transition (at 750 K), the correlation sharply decays to zero across the transition, within several picoseconds at 850–900 K. Also, the ACF's decay progressively more rapidly at higher temperatures. The correlation time (obtained from the time integral of ACF) at 1000–1400 K is found to be of the order of $10^{-13}$ s. It indicates that there is some correlation in time between the phases $\alpha_1$ and $\alpha_2$, apart even temporarily (over $10^{-13}$–$10^{-12}$ s), in the high-temperature $\beta$ phase. Note that the above process is much slower than the initial rapid decay of the order of $10^{-14}$ s, which is associated with local dynamics due to the atomic

vibrations within $SiO_4$ tetrahedra, i.e., stretching of the Si-O bonds; antisymmetric or symmetric Si-O stretch modes correspond to 33–36 THz or 21–24 THz, respectively.[16] Moreover, the effect of these high-frequency atomic vibrations to the phase-mixing dynamics is negligible, even at 1400 K. Thus, we confirm that the dynamical phase-mixing behavior in the $\beta$ phase is dominated by the intertetrahedral $SiO_4$ vibrations; torsional $SiO_4$ modes, and intratetrahedral bending modes lie between ca. 3.0 and 16.5 THz.[16] This fact coincides with the existence of low-energy rigid-unit-mode motions in quartz (typically of the order of 1 THz or less), which are natural candidates as soft modes for displacive instabilities (see, for example, Ref. 17).

## V. CONCLUSIONS

In conclusion, our MD approach based on the BKS pairwise potential permits a coherent description of the marked changes with temperature in the elastic properties of quartz, including the $\alpha$-$\beta$ structural phase transition. In particular, the characteristic temperature dependence of the elastic constants above the transition, i.e., a saturated growth after a discontinuous increase, is well described by the stress-fluctuation-term contribution to the elastic constants, which arises from the internal relaxations as a consequence of the cooperative motions of corner-linked $SiO_4$ tetrahedra. Our simulations reveal the effect on elastic properties of dynamical organization of neighboring $SiO_4$ tetrahedra and the local heterogeneity in the $\beta$ phase. We show that the $\beta$ phase is realized as a dynamically averaged structure, which depends on the time and length scales of the disordered structure with small-$\alpha$ domains, as a function of temperature. To this end, our simulations provide a different microscopic insight into the intimate relation between the macroscopic elastic behavior and the nature of dynamical disorder present in the high-temperature phase of quartz.

## ACKNOWLEDGMENTS

The authors express appreciation to S. Yip and D. Liao for useful discussion on the methodology of the MD simulations of $SiO_2$ systems.

*Electronic address: kimizuka.hajime@jri.co.jp

[1] J.V. Atanasoff and P.J. Hart, Phys. Rev. **59**, 85 (1941); J.V. Atanasoff and E. Kammer, *ibid.* **59**, 97 (1941); E.W. Kammer, T.E. Pardue, and H.F. Frissel, J. Appl. Phys. **19**, 265 (1948); V.G. Zubov and M.M. Firsova, Kristallografiya **7**, 469 (1962) [Sov. Phys. Crystallogr. **7**, 374 (1962)]; H. Unoki, H. Tokumoto, and T. Ishiguro, in *Phonon Scattering in Condensed Matter*, edited by W. Eisenmenger, K. Lassmann, and S. Döttinger (Springer-Verlag, Heidelberg, 1984), p. 292; I. Ohno, J. Phys. Earth **43**, 157 (1995).

[2] M.A. Carpenter *et al.*, Am. Mineral. **83**, 2 (1998).

[3] M.B. Smirnov and A.P. Mirgorodsky, Phys. Rev. Lett. **78**, 2413 (1997); M.B. Smirnov, Phys. Rev. B **59**, 4036 (1999).

[4] S. Tsuneyuki, M. Tsukada, H. Aoki, and Y. Matsui, Phys. Rev. Lett. **61**, 869 (1988); S. Tsuneyuki, H. Aoki, M. Tsukada, and Y. Matsui, *ibid.* **64**, 776 (1990).

[5] G. Dolino and J.P. Bachheimer, Ferroelectrics **43**, 77 (1982).

[6] R.A. Young, U.S. Air Force (Office of Scientific Research) Report No. 2569, 1962 (unpublished).

[7] A.F. Wright and M.S. Lehmann, J. Solid State Chem. **36**, 371 (1981).

[8] S. Nosé, Mol. Phys. **52**, 255 (1984); W.G. Hoover, Phys. Rev. A **31**, 1695 (1985).

[9] M. Parrinello and A. Rahman, J. Appl. Phys. **52**, 7182 (1981).

[10] B.W.H. van Beest, G.J. Kramer, and R.A. van Santen, Phys. Rev. Lett. **64**, 1955 (1990).

[11] M. P. Allen and D. J. Tildesley, *Computer Simulation of Liquids* (Oxford University Press, Oxford, 1989).

[12] J.R. Ray, M.C. Moody, and A. Rahman, Phys. Rev. B **32**, 733 (1985); J.R. Ray, Comput. Phys. Rep. **8**, 109 (1988).

[13] H. Kimizuka, H. Kaburaki, and Y. Kogure, Phys. Rev. Lett. **84**, 5548 (2000).

[14] R. Bechmann, Phys. Rev. **110**, 1060 (1958).

[15] E.W. Kammer and J.V. Atanasoff, Phys. Rev. **62**, 399 (1942).

[16] G.J. Kramer, N.P. Farragher, B.W.H. van Beest, and R.A. van Santen, Phys. Rev. B **43**, 5068 (1991).

[17] S.A. Wells, M.T. Dove, M.G. Tucker, and K. Trachenko, J. Phys.: Condens. Matter **14**, 4645 (2002).